Simulation of laser beam propagation over land and sea using phase screens – a comparison with experimental data

Lars Sjöqvist[‡], Markus Henriksson and Ove Steinvall

Dept. of Laser Systems, Swedish Defence Research Agency, FOI
P.O. Box 1165, SE 581 11, Linköping, Sweden

ABSTRACT

Understanding and predicting laser beam propagation effects in the atmosphere is of importance for laser countermeasures and related applications. Turbulence effects cause beam wander, beam broadening and intensity scintillations reducing e.g. the power in bucket and the tracking accuracy. Modelling laser beam propagation in turbulence using successive phase screens provides an efficient tool for performance predictions. In this work phase screens are used to model laser beam propagation over land and sea. Different phase screens generators utilising the Kolmogorov or von Karman spectra were considered. Critical parameters using phase screens include the number of screen applied along the propagation path, inner- and outer scale size, variations in the structure parameter and spatial frequencies. Effects such as beam wander, angle-of-arrival fluctuations and intensity scintillations are discussed. The simulated results are compared with experimental data recorded at different ranges, various turbulence strengths and for single- and double paths. A generic example describing laser countermeasure against an infrared homing missile in a naval scenario is presented.

Key words: Laser, propagation, turbulence, countermeasures, numerical, model, phase screens.

1. INTRODUCTION

Atmospheric turbulence effects may have strong influence on the performance of several military laser applications such e.g. laser countermeasures, active imaging and free-space optical communication. Laser countermeasures, including directed infrared countermeasures (DIRCM) and electro-optical countermeasures (EOCM), have attracted considerable interest during recent years. One important task considering military and civilian airborne platforms is to protect the platform from heat seeking missiles by DIRCM techniques. The turbulence effects introduce laser beam broadening, beam wander and intensity variations (scintillations) causing degradation in performance parameters such as; power (energy) on target, detection range and tracking accuracy. Temporal effects due to turbulence induce fading and may affect jam sequences. Modelling atmospheric turbulence effects provides an efficient tool for predicting the performance of the laser countermeasures techniques. Analytical models can be utilised for fast estimates of the influence from perturbations originating from turbulence. Several excellent monographs are available in the literature treating the subject comprehensively[1]. Using numerical methods based on physical optics provides, on the other hand, additional information about the laser beam properties which is of importance in performance predictions focusing on the transversal profile and behaviour of the phase of the optical field. Using numerical methods the overall system performance can be modelled including the laser system, the atmospheric path and target properties.

Numerical beam propagation methods are commonly used to model adaptive optics, imaging and laser beam propagation problems describing the propagation of the optical field through a turbulent atmosphere[2]. Simulations of three-dimensional (3D) wave propagation through randomly varying media have been described in detail previously[3,4]. Details about principles and the propagation algorithm, critical parameters, accuracy and limitations were discussed. Inclusion of time dependent effects originating from atmospheric turbulence have also been suggested[5,6]. Belmonte

‡) email: larsjo@foi.se

Technologies for Optical Countermeasures II; Femtosecond Phenomena II; Passive Millimetre-Wave & Terahertz Imaging II,
ed. by D.H. Titterton, S.M. Kirkpatrick, R. Stoian, R. Appleby, J.M. Chamberlain, K.A. Krapels,
Proc. of SPIE Vol. 5989, 59890D, (2005) · 0277-786X/05/$15 · doi: 10.1117/12.630655

have studied the feasibility of numerical beam propagation in view of application to coherent lidar[7]. Analytical theories developed to describe relevant parameters of laser beam propagation in a turbulent atmosphere were compared with results from numerical simulations. In general, studies comparing numerical beam propagation schemes with experimental data seem to be less frequently reported. Parameters used in the modelling scheme may limit its applicability to comparison with experimental data.

Long term experimental studies of the atmospheric turbulence effects on laser beam propagation is of importance to relate environmental parameters to beam propagation effects and estimate magnitudes of perturbations which degrade the performance of laser systems. Quantifying the magnitude of atmospheric turbulence experimentally at various metrological conditions is valuable in evaluation of models. Important parameters include e.g. the order of magnitude of turbulence, weather conditions, propagation length, single and double path effects and the environment (e.g. close to the sea surface or ground). Long-term measurements have been carried out in a sea environment (in the Baltic sea) at different ranges and over ground using a low altitude propagation path studying parameters such as e.g. amplitude characteristics, fading and tracking behaviour[8,9,10]. In a recent reported study scintillation effects were registered experimentally for different receiver apertures using a horizontal propagation path and compared with theoretical results[11]. Laser beam propagation in an Middle East environment have been studied by Bendersky and coworkers[12,13]. They developed a model based on meteorological data for estimating variations in the structure parameter. In addition, scintillation features and fading probabilities in a double path propagation path were recently considered[14].

In this work results from numerical propagation using the angular spectrum method and application of successive phase screens were compared with experimental data recorded over sea and land. The results show that numerical beam propagation methods can be used to predict perturbations originating from atmospheric turbulence and, hence, be used in performance modelling of military laser system such as e.g. laser countermeasures.

2. Theory

Beam propagation methods are used to numerically study effects due to diffraction and perturbations which can be described in terms of phase variations. In 3D models the transversal extent of the optical (electrical) field is represented by a complex matrix containing the amplitude. By solving the paraxial wave equation propagation of plane waves can be expressed in terms of the angular spectrum[15]. Propagation along the *z*-axis is in this scheme represented by the Fresnel operator. The angular spectrum method can be realised by using numerical methods based on the discrete Fourier transform (DFT) since the propagation operation is represented by a multiplication of the field with the Fresnel operator in the frequency domain. An inverse DFT provides the field after propagation. The advantage of this scheme is the fast operation of the DFT using relative large matrices for field representation. Perturbation effects, such as those induced by atmospheric turbulence, can be incorporated by a split-step method treating propagation and phase perturbations separately and in discrete steps along the propagation axis. The phase perturbations caused by refractive index fluctuation arising from turbulence effects are implemented by multiplying the field by a phase exponential function in each step. This scheme is commonly referred to as the method of successive phase screens and has been applied to various applications such as e.g. long-range imaging, adaptive optics or free-space optical communication through the atmosphere[2].

2.1. Spectral models

Turbulence effects in the atmosphere alter the refractive index in a random manner due to temperature fluctuations. Several spectral models have been considered describing the statistical behaviour of the refractive index variations and in this paragraph the most commonly used models in numerical beam propagation methods are briefly summarised. The spectrum derived by Kolmogorov serves as foundation for describing the spatial variations of the refractive index in a turbulent atmosphere

$$\Phi(\kappa) = 0.033 C_n^2 \kappa^{-\frac{11}{3}} \tag{1}$$

where κ is the spatial frequency and C_n^2 the structure parameter. The Kolmogorov spectrum is valid in the inertial sub range limiting the spatial frequencies to $\frac{2\pi}{L_0} \le \kappa \le \frac{2\pi}{l_0}$ where L_0 and l_0 denote the outer- and inner scales of the turbulence, respectively. The outer scale length defines the largest turbulence cells (usually non-homogeneous) and is believed to be of the order 10 to 100 m for atmospheric turbulence. The inner scale, on the other hand, is assigned the spatial range where the turbulence cells are dissipated into heat and can be smaller than 1 cm. The Kolmogorov spectrum contains singularities at high and low spatial frequencies which introduce problems in phase screen generation. These singularities can be removed by introducing the von Karman modification which is expressed as

$$\Phi(\kappa) = 0.033 \frac{e^{-\frac{\kappa^2}{\kappa_m^2}}}{\left(\kappa^2 + \kappa_0^2\right)^{11/3}} \tag{2}$$

where $\kappa_m = \frac{5.92}{l_0}$ and $\kappa_0 = \frac{2\pi}{L_0}$. The κ_0 and κ_m terms in eq. (2) removes the infinity behaviour at low frequencies and introduces a frequency cut-off at higher frequencies. In addition to the von Karman spectrum an additional spectrum frequently considered is the Hill Spectrum

$$\Phi_n(\kappa, z) = A C_n^2(z) \kappa^{-11/3} f[\kappa l_0] \tag{3}$$

where $A = 0.0330054$ and l_0 is the inner scale size. The polynomial function is defined according to $f(x) = \left(1 + 0.70937x + 2.8235x^2 - 0.28086x^3 + 0.08277x^4\right) e^{-1.109x}$. The variation of the power spectral density (PSD) as a function of spatial frequency for the described spectra is depicted in Figure 1.

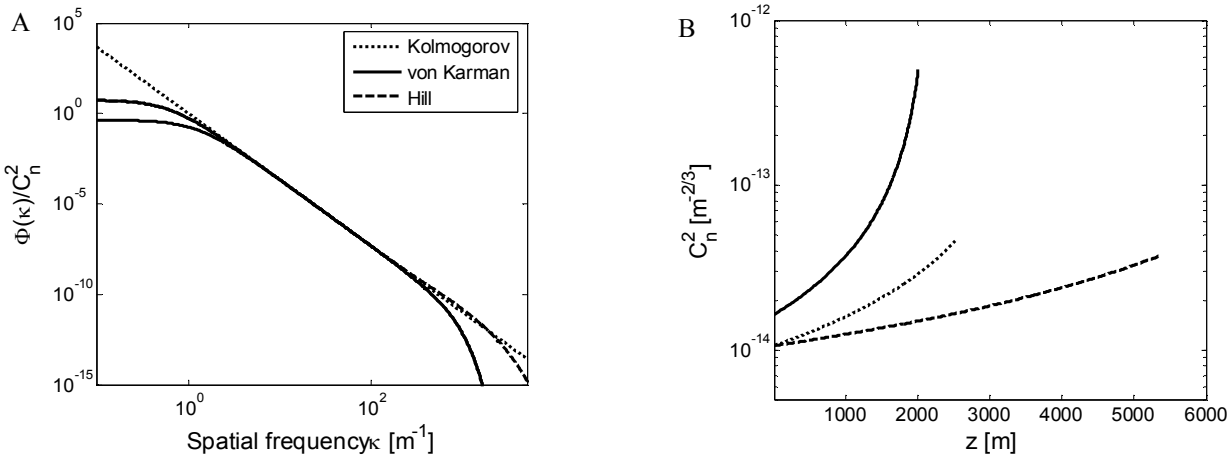

Figure 1: A) Spectra representing refractive index fluctuations due to atmospheric turbulence. The decrease in the PSD at lower spatial frequencies can be observed for the von Karman and Hill spectra. The inner scale was l_0 = 1cm and the outer scale L_0 = 10 or 5 m. The PSD decreases when the outer scale increases using the von Karman spectrum. B) Estimated variation of C_n^2 using eq. (5) for distances L = 2000 (solid-ground), 2520 (dotted-sea) and 5360 (dashed-sea) m with initial heights H_1= 18 (sea), 11 m (ground) and end heights H_2 = 6 (sea), 8 (sea) and 1m (ground), respecively.

The relation between the spectrum of the spatial varying phase screen (used in the angular spectrum propagation method) and the spectrum of the refractive index variations is given by

$$\Phi_\theta(\kappa) = 2\pi k^2 \Delta z \Phi_n(\kappa) \tag{4}$$

where k is the wave vector and Δz is the thickness of the turbulence layer.

All spectral representations described above were implemented in the phase screen generators. However, only von Karman and Hill representation are utilised since the Kolmogorov spectrum is known to cause a cyclic when generating phase screens with FFT methods[16].

2.2. Turbulence model

The strength of turbulence along the propagation path is described by the structure parameter C_n^2. Several models for predicting the variation of the structure parameter as a function of height, wind speed and meteorological parameters have been suggested, see e.g. refs[2,12,13]. The parameter having the strongest influence on the magnitude of the structure parameter is the altitude. Choosing an appropriate model for the structure parameter variation is usually a delicate task depending critically on the surrounding environment and the propagation geometry.

In this work we choose simple exponential height dependence (an approximation for day time turbulence) and evaluate the variation in the structure parameter along the nearly horizontal path. The variation in the structure parameter can then be described using Tatarski's model

$$C_n^2(h) = C_n^2(h_0)\left(\frac{h}{h_0}\right)^{-4/3} \tag{5}$$

where h_0 defines a reference height and we assume that $C_n^2(h_0 = 1) = 5 \cdot 10^{-13}$ m$^{-2/3}$. The experimental data used corresponds to a propagation distances L = 2.5 and 5.4 km having the laser system at 18 m height and the targets at 6 and 7 m height for propagation paths over sea. The ground path was L = 2 km and laser at 13 m height and target 1 m above the ground. If we use eq. (5) the variation in the structure parameter can be estimated for the sea and ground paths, respectively (Figure 1B). We approximate the structure parameter to be constant along the nearly horizontal path over sea. Although this simple model was mainly used in this work a varying C_n^2 can easily be incorporated in the simulations by changing the value applied for each discrete turbulence layer according to the chosen C_n^2 model. Considering the ground path the magnitude of the structure parameter varies more significantly and this simple model must be viewed as a first approximation.

In addition to the structure parameter we can also use Fried's parameter, r_0 (or the seeing cell size), in describing the turbulence variation along the propagation path. Fried's parameter is related to the integrated structure parameter

$$r_0 = 0.185\left[\frac{4\pi^2}{k^2\int_0^L C_n^2(z)\,dz}\right]^{3/5} = 0.185\left[\frac{4\pi^2}{k^2\sum_{i=1}^{N} C_{n_i}^2 \Delta z_i}\right]^{3/5} = \left[0.421k^2\sum_{i=1}^{N} C_{n_i}^2 \Delta z_i\right]^{-3/5} \tag{6}$$

where the summation indicates the scheme implemented in this work with the structure parameter (or r_0) determining the turbulence strength within the layer. Alternatively we can express the turbulence strength in terms of an effective Fried's parameter according to $r_{tot} = \left[\sum_{i=1}^{i=N} r_{0,i}^{-5/3}\right]^{-3/5}$.

2.3. Phase screen generation

An important part of numerical beam propagation through a turbulent medium using the angular spectrum method is the generation of phase screens. Several different approaches have been suggested and they exhibit both advantages and drawbacks. In the case of performance modelling of e.g. laser countermeasure systems the time and computational power to generate phase screens are important. The phase screen generating methods can be divided into two different approaches using a modal representation expressed in appropriate basis functions or a direct generation using discrete grid and generate the phase screen from the given spectrum based on FFT techniques[2].

Generation of FFT based phase screens to mimic the statistical behaviour of the phase fluctuations due to a turbulent atmosphere was proposed by McGlamery[17]. This scheme was analysed in more detail for non-Kolmogorov phase screens[18]. One of the shortcomings using the FFT method is the inability to represent spatial frequencies of lower magnitude responsible for the lower aberration such a tilt. Improvement of the FFT method has been suggested by incorporating sub harmonics in the scheme[19]. Moreover, recently a method for implementation of large FFT generated phase screens was suggested by Sedmak[20]. A fast phase screen simulation method based on the covariance methods has been described in the literature[21].

In modelling laser countermeasures three different methods have been implemented. The simplest method utilises a standard scheme based on FFT generation whereas a set of randomly (following a Gaussian distribution) complex numbers are generated on the chosen grid e.g. N = 1024x1024. The random numbers are multiplied with the square root of the spectral function (properly scaled) and an inverse FFT gives the phase screen. Two independent screens are generated for each calculation. This method provides a rapid generation of two phase screens.

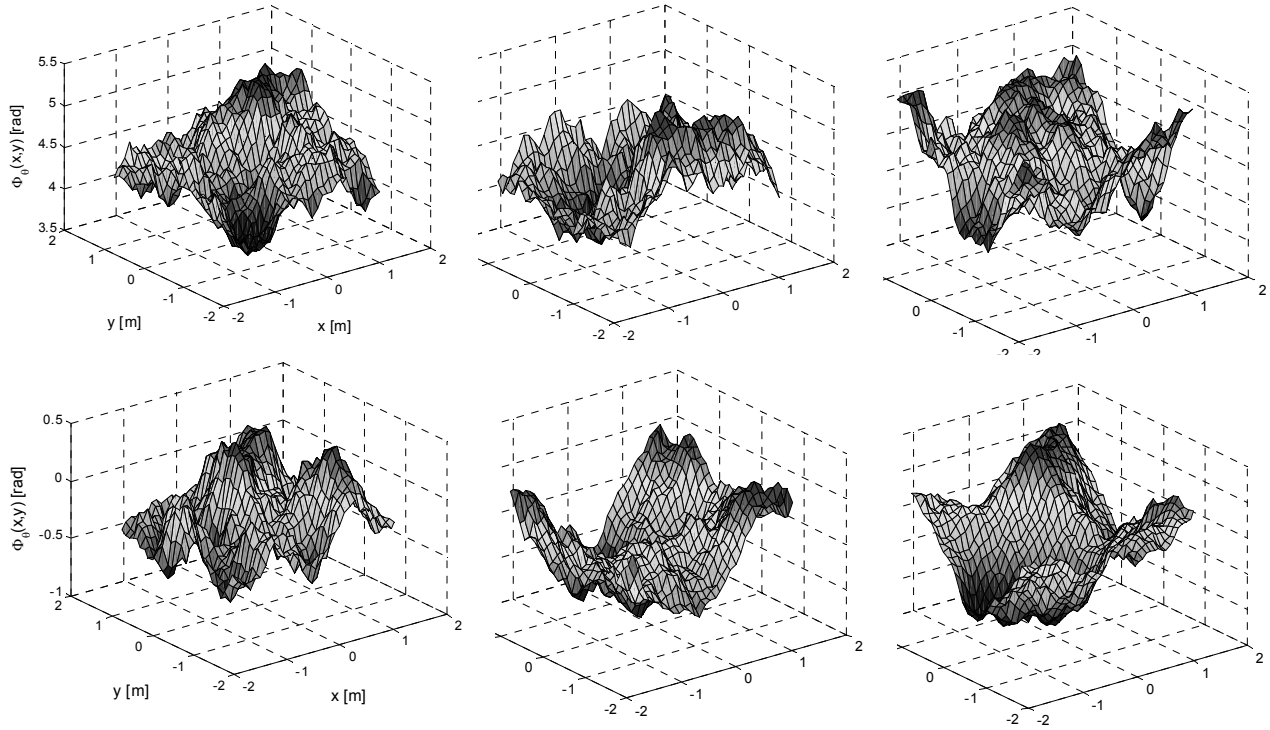

Figure 2: Example of randomly generated phase screens corresponding to $C_n^2 = 1 \cdot 10^{-13}$ m$^{-2/3}$, L_0 = 10 m and Δz = 250 m. The screen size was 250 cm using 2048x2048 points. The screens were generated using the FS generator with 300 Fourier components (three upper) and with the FFT scheme (three lower) using the von Karman spectrum and neglecting the inner scale parameter.

In addition we use a modal method based on a Fourier-Series (FS) expansion of the spectral content which has been developed by Welsh[22]. A vector-based equation was derived providing a fast method to calculate the phase screens. The advantage of the FS approach, in comparison to methods using the discrete Fourier transform, is the capability to represent the part of the spectrum containing low spatial frequencies. The part of the spectrum containing lower spatial frequencies give raise to large order phase perturbations introducing tip/tilt errors and wandering of the centre of gravity of the beam. Temporal effects from a cross wind vector were implemented using the FS method. The high frequency content in the generated screens can be controlled by altering the number of coefficients in the FS. The strength of the turbulence is controlled by the structure parameter C_n^2 (or *r0*) and the effective length of the turbulent zone. Example of phase screens generated using the FS and FFT methods are depicted in Figure 2.

The phase screens were generated using random numbers and up to 128 phase screens were generated to obtain a statistical data set and grid sizes up to 2048x2048 were tested. The phase screen generators were implemented using MATLAB. The numerical propagation was performed using a commercial software with a accompanying phase screen generator[23]. A Matlab based propagation module was also available and used on some occasions. The phase screen generators and the propagation routines were executed on a PC work station using two 2.3 GHz Pentium4 processors. A benchmark test using the following parameters: 1024x1024, 128 independent phase screens, field size 1x1 m, 300 FS components resulted in computation times of 216 and 20 s for the FS and FFT methods, respectively. It should be noted that the computational time required for the FS scheme depends on the number of included FS components.

2.4. Turbulence effects

The effects related to atmospheric turbulence which needs to be considered include beam broadening, beam wander, angle of arrival fluctuations and intensity scintillations. Since beam broadening was not considered in the experimental data we neglect it in this work. The beam wander, or centroid motion, can be expressed as[1]

$$\left\langle \sigma_c^2 \right\rangle \simeq \frac{2.97 z^2}{k^2 \rho_0^{5/3} D_b^{1/3}} \tag{7}$$

where z is the propagation distance, $\rho_0 \approx 2r_0$ is the transversal coherence length and D_b the beam aperture diameter. The scintillation, or intensity fluctuations, related to atmospheric turbulence is expressed in terms of the scintillation index (or normalised variance of the intensity fluctuations)

$$\sigma_I^2 = \frac{\left\langle I^2 \right\rangle}{\left\langle I \right\rangle^2} - 1 \tag{8}$$

where I denotes the intensity and the brackets is the ensemble average. The scintillation index can be estimated for weak (and moderate) turbulence using the Rytov approximation valid for plane wave (constant $K = 1.23$)

$$\sigma_I^2 = K \cdot C_n^2 k^{7/6} L^{11/6} . \tag{9}$$

In addition, angle of arrival phase fluctuations due to phase variations in front of the aperture cause image motion in the focal plane. The rms value of the angle of arrival fluctuations can be estimated by the following expression[1]

$$\left\langle \beta^2 \right\rangle = \frac{\left\langle (\Delta S)^2 \right\rangle}{(k D_r)^2} \tag{10}$$

where ΔS denotes the total phase shift across the receiver aperture (with diameter D_r) and k the wave vector.

3. EXPERIMENTAL METHOD

The experimental data sets used in this study were registered on several occasions using propagation paths over sea and land. Details about the experimental equipment and the measurement procedures have been presented previously[8,9,10]. In this paragraph the experimental method is summarised focusing on recorded data utilised in the comparison with the numerical simulations shown below.

The laser system consisted of a CO_2 laser integrated with an acquisition, tracking and pointing (APT) assembly. The receiver channel uses Cassegrain optics (150 mm in diameter) and a quadrant detector for active tracking and recording of temporal resolved targets. The laser is pulsed with a peak power of 600 W and pulse durations of 70 or 8 μs @ 2 or 25 kHz, respectively. The wavelength was 10.6 μm with a beam divergence of 1 mrad. The beam profile was close to a Gaussian distribution. The typical registration period was 7 s long @ 2 kHz sampling rate. Three different propagation lengths were used in the measurements over sea. Here, the ranges were L = 2.52, 5.36 and 16.65 km. Corner cubes were used as targets and located on islands at heights 6, 7.5 and 11.5 above the sea surface and the laser system was placed at 18 m height above sea level. The corner cubes had the diameters, 1.3, 2.5 and 6.35 cm. In addition to corner cubes a

receiver consisting of a lens having an aperture of 50 mm in diameter and an un-cooled MCT detector located in the focal plane of the lens was used for simultaneous single- and double path registrations (Figure 3). The single path receiver signal was down-sampled to 2 kHz with a peak detector. The experimental data was post processed off-line. Registrations of the turbulence strength were performed using a scintillometer (Scintec AG BLS900) operating at 880 nm wavelength. The Scintillometer was placed at distances 2.5 or 5.4 km in the sea measurements.

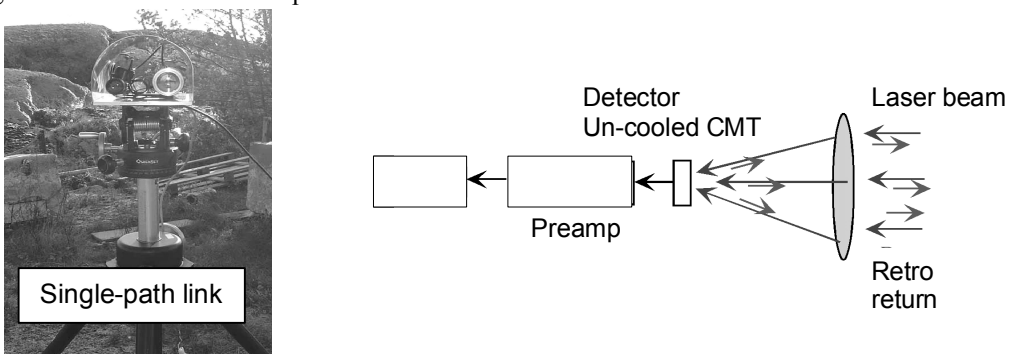

Figure 3: Photograph showing the single path receiver used in sea measurements at L = 5.5 km and in ground measurements at L = 2 km (left). The receiver contained a collecting lens and a CMT detector with corresponding preamplifier (right). An external PC was used for data acquisition and storing of single path data sets.

In the recording of data using the nearly horizontal path over ground the distance was L = 2 km and the laser system was located 11 m above ground while the single path receiver was 1 m above ground. Registration of turbulence effects were measured at different times during the day (and night) at several occasions. In comparisons with simulated results data points from the experimental sets far enough in time to be uncorrelated were chosen.

4. RESULTS

4.1. Experimental results

In this section some illustrative results from the measurement campaigns are presented. Although the experimental study resulted in a large database we choose to focus on the experimental results involving the single path link receiver in this work. Moreover, results from the longest distance, L = 16.6 km, was not included in the analysis due to limitations in the spatial resolution of the simulations dictated by the experimental conditions. The discussion covered by the numerical model is concentrated on the amplitude data i.e. considering intensity scintillations. In addition, angular fluctuations are briefly discussed.

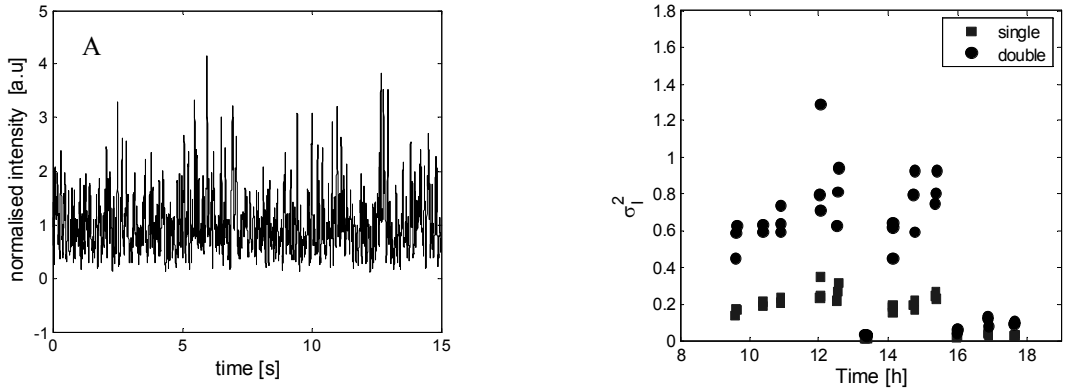

Figure 4: A) Representative signal registered using the single path receiver described above corresponding to $\sigma_I^2 = 0.28$ at L=5.5 km distance over sea. B) Example of variation of the scintillation index for simultaneous registered single and double path signals over ground at L = 2 km distance.

The variance in signal intensities varied between $\sigma^2_{I,\text{single}} \sim 0.01$ to 0.8 and $\sigma^2_{I,\text{double}} \sim 0.01$ to 4.5 for single- and double path registrations performed with the single path link close to the sea surface (L = 5.5 km). The corresponding intensity fluctuations observed during propagation above ground was $\sigma^2_{I,\text{single}} \sim 0.01$ to 0.4 and $\sigma^2_{I,double} \sim 0.01 - 0.9$ for the single and double path intensity variance, respectively. A representative signal registered during propagation close to the sea surface is depicted in Figure 4A. In Figure 4B an example of variations in scintillation index for simultaneously recorded single and double path signals is presented. The observed experimental intensity scintillations correspond to a representative variation in Fried's parameter from 8 to 50 cm in a single path and 5 to 25 cm in a double passage channel, respectively.

The experimentally observed angle of arrival fluctuations data were obtained by disconnecting the tracker and registering the fluctuations on the quadrant detector at different metrological conditions. The observed fluctuations varied between 20 and 70 μrad @ 2.5 and 5.5 km distance in turbulence strengths corresponding to a structure parameter in the range $C_n^2 = 1 \cdot 10^{-13}$ to $1 \cdot 10^{-14}$ m$^{-2/3}$ for sea registrations. The corresponding values for the ground path were 20 to 140 μrad.

4.2. Numerical simulations

In the simulations experimental scintillation values were used to determine the magnitude of the structure parameter (or r_0) using the Rytov expression. Additionally, data from the scintillometer measurements were utilised when they have been recorded. The value of the structure parameter used in the simulations was adjusted to scintillometer readings and corrected for aperture averaging [10]. In the comparison of signal fluctuations the experimental data sets were re-sampled to contain un-correlated samples relevant for comparison with the numerically simulated data.

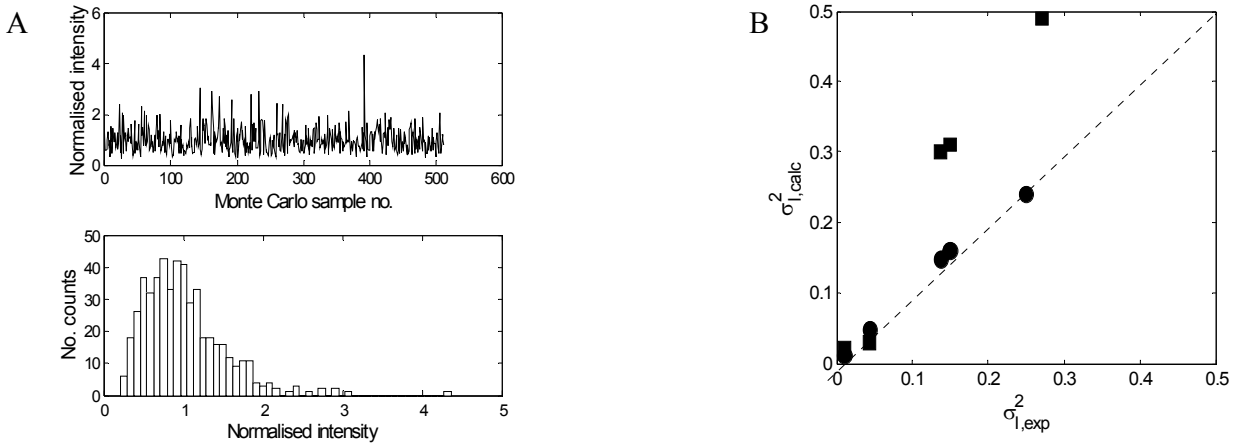

Figure 5: A) Example showing the fluctuation (uncorrelated samples) about the mean at L = 2 km single path propagation, $C_n^2 = 1 \cdot 10^{-13}$ m$^{-2/3}$ and number of phase screens N_{ps} = 8. The corresponding scintillation index is $\sigma_I^2 = 0.28$. The lower graph depicts probability distribution of the signal. B) Experimental and calculated scintillation index for single path propagation. The same parameters as in A) were used. Correction factor from scintillometer data (squares) and adjusted to fit experimental data (circles).

In Figure 5A an example showing the variation in the calculated intensity corresponding to a 2 km propagation path above ground is illustrated. The distribution function of the signal fluctuations exhibit a lognormal appearance as expected in weak to moderate turbulence strength. Two ways to estimate the strength of the turbulence were employed for comparing experimental scintillations with calculations. The method based on corrected scintillometer readings seems to overestimate the scintillation index while adjusting the constant in eq. (9) to K = 3 to fit an experimental data set gives good agreement if the turbulence is varied (Figure 5B). Using a larger value for the constant the intensity scintillations at stronger turbulence seem to be exaggerated. The capability of the FS method to handle lower spatial frequencies is also manifested by the increase in beam wander. As an example the beam wander was calculated to be 17 μrad rms at L = 2 km assuming $C_n^2 = 0.5 \cdot 10^{-14}$ m$^{-2/3}$ which is in agreement with estimates using eq. (7).

In Figure 6A another example comparing the signal variations from an experimental registration with calculations at 2 km range is presented. In this case the experimental time series was re-sampled to approximately correspond to uncorrelated samples. The simultaneously recorded (or calculated) single- and double path intensity fluctuations are shown. The corresponding scintillation indexes were $\sigma^2_{I,\text{single}} = 0.044$ and $\sigma^2_{I,\text{double}} = 0.13$ for the experimental data and were $\sigma^2_{I,\text{single}} = 0.055$ and $\sigma^2_{I,\text{double}} = 0.12$ for the simulations. The fluctuations observed experimentally exhibit a less fluctuating signal in comparison to the calculated fluctuations suggesting that successive points still are correlated. In addition to calculations performed at L = 2 km tests were also performed for the longer propagation distances corresponding to L = 2.5 and 5.5 km. The model could also reproduce experimental results obtained at longer distance. However, the decreased spatial resolution introduces larger uncertainties in the calculated parameters.

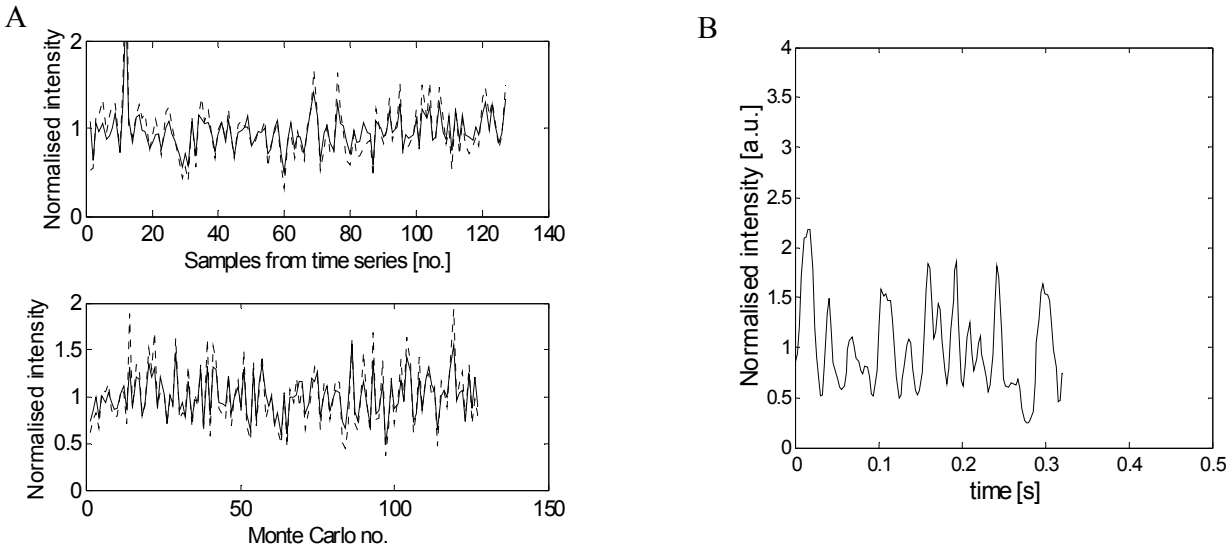

Figure 6: A) Experimental (upper) and calculated uncorrelated (lower) intensity variations for simultaneously registered single (solid line) and double path signals (dotted line) at L = 2 km, N_{ps} = 4 and 1024x1024 grid. The sampling interval of the experimental data was Δt = 32 ms. B) Calculated time correlated signal corresponding to the following parameters: single path L = 2 km, N_{ps} = 8, Δt = 25 ms, $C_n^2 = 1 \cdot 10^{-14}$ m$^{-2/3}$, crosswind = 5 m/s. The FS phase screen generator was used.

An example illustrating how a time-correlated signal can be calculated using the FS method is shown in Figure 6B. Here, the number of phase screens was limited to N_{ps} = 8 and the effective structure parameter were taken to be $C_n^2 = 1 \cdot 10^{-14}$ m$^{-2/3}$ for single path propagation.

In order to investigate the influence from the phase screen generator the scintillation index was calculated for fixed parameters (N_{ps} = 8, L = 2 km, $C_n^2 = 1 \cdot 10^{-13}$-$1 \cdot 10^{-14}$ m$^{-2/3}$) varying only the used generator (FFT or FS). The results show that the FS based phase screen generator gives higher scintillation index (between 40 to 60 %) due to the contribution from lower spatial frequencies. The FFT phase screen generator neglects low frequency content in the spectrum lowering the influence from tip-tilt errors while the FS method take this contribution into account[22]. One advantage of using a FFT based screen generator is the capability of creating two independent phase screens for each realisation[17]. This feature increases the speed of the calculations when a large number of Monte Carlo simulations are performed.

4.3. A laser countermeasure example

The model described above can be utilised to study the performance of optical countermeasures. The influence from atmospheric turbulence may severely degrade the performance of an optical countermeasure system in presence of strong turbulence and at long range. Numerical beam propagation methods can be used to model the laser system, the atmospheric channel and target effects. In addition, compensation schemes invoked by adaptive optics can also be

analysed. In this generic example the effects of atmospheric turbulence is illustrated for a laser countermeasure system acting against a heat seeking missile in a naval environment. The wavelength was chosen to $\lambda = 4$ μm (phase screens were scaled by using eq. (4)) representing a laser countermeasure system operating in mid-ir. The typical parameters used in the simulation are presented in Table 1.

Table 1 Laser countermeasure system and target parameters used in the calculations

Laser	**Value**	**Target**	**Value**
Laser power	5 W, beam diameter 25 mm	Diameter	6 cm, 5% reflectivity
Wavelength	4 μm	**Atmospheric channel**	**Value**
Mechanical jitter	50-150 μrad rms	Turbulence C_n^2	$1x10^{-13}$-$1x10^{-15}$ $m^{-2/3}$
Beam divergence	0.3 or 0.6 mrad	Range	5 km
Transceiver aperture	8 cm (diameter)		
Detector NEP	1 nW @20 kHz bandwidth		

One important parameter considering performance of a laser countermeasure system is the average power entering the target aperture commonly denoted "power in bucket" (PIB). The PIB determines the jammer to signal (JSR) ratio in case of a jamming system. Temporal fluctuations due to turbulence may affect the jam sequence and the ability to break-lock. In Figure 7A is an example of the calculated PIB as a function of turbulence strength and distance between the target and the laser system depicted.

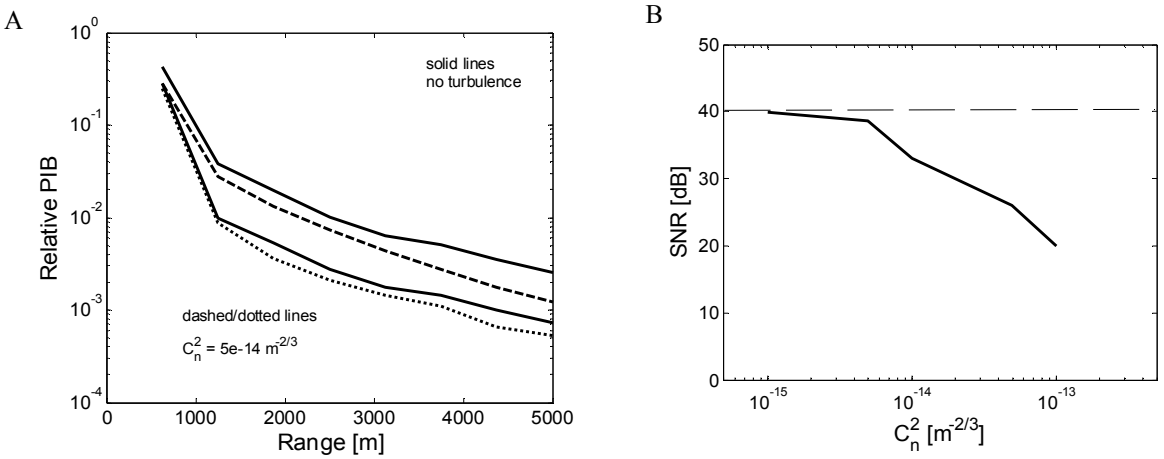

Figure 7: A) Calculated average relative power in bucket (PIB) as a function of propagation distance and beam divergence (300 μrad-dashed, 600 μrad-dotted). The following parameters were used: N_{ps} = 8, 512x512 grid, 64 Monte Carlo realisations and the FS phase screen generator. B) Calculated retro signal (signal to noise ratio, SNR) from target at 5 km distance as a function of turbulence strength. The dashed line corresponds to the calculated SNR in presence of no turbulence. The same parameters as in A) were used, see also Table 1.

In this generic example it is assumed that the approaching infrared missile is close to the sea surface motivating the use of experimental parameters to tune the model. The laser countermeasure system is located on a naval platform ca. 15 m above the sea surface. In Figure 7B the calculated retroreflected signal from the approaching target is depicted. A 20 dB reduction in the retroreflected signal is calculated at 5 km distance. In this calculation a simple model corresponding to a corner cube represented the target. However, more complicated optics can be taken into account. The results show that turbulence effects need to be considered in order to obtain optimal signal to noise ratio for tracking on the retro signal. In addition, a jitter term was also added to the model permitting which decreased the instantaneous SNR or relative PIB.

5. DISCUSSION AND CONCLUSIONS

Numerical beam propagation methods can advantageously be utilised in predicting performance of laser countermeasure and similar systems. The advantage of using numerical methods includes information about spatial and phase properties

of the beam can be extracted. This information is of importance when judging the impact and effects of compensation techniques using active (adaptive) optics. In addition to turbulence effects beam jitter arising from the system or platform may be implemented by choosing an appropriate statistical model. Numerical beam propagation studies may also be used to derive probability density functions which may be approximated analytically and used for performance and system utility predictions with the help of meteorological statistics[24].

One important issue in numerical simulations using phase screens is the choice of an appropriate spectral model. The selected model and magnitude of chosen outer and inner scale length affects the generation of the phase screens since the amplitude weighting depends on the power spectral density of the phase fluctuations. The experimental setup should also be carefully designed so that an appropriate resolution is obtained. In this study we showed that experimental results could be reproduced to an acceptable degree of accuracy providing a tool for predicting the performance of laser countermeasures in a turbulent atmosphere. Critical parameters included the chosen spectral model and the resolution limiting the spatial frequency content.

The method of successive phase screens provides additional information to performance calculation including effects due to beam wander, angle of arrival fluctuations and intensity scintillation. The major drawback with the method is the computational time required in problems involving large grids and a strongly varying structure parameter along the path which necessitates the use of a large number of phase screens.

In conclusion, numerical laser beam propagation calculations were compared with experimental data describing degradation effects due to a turbulent atmosphere. It was possible to reproduce the experimental results by adjusting model parameters to a single set of the experimental data. Although the approximate approach of a constant structure parameter along the path due to the nearly horizontal geometry was used here a varying structure parameter can easily be implemented taking slant paths into consideration. Systematic studies of the experimental data sets are to be conducted in future studies. The results encourage the use of phase screen methods in modelling laser countermeasure systems.

ACKNOWLEDGEMENT

This work was funded by the Swedish Armed Forces head quarter and the Swedish Defence Materiel Administration (FMV).

REFERENCES

[1] See e.g. V.I. Tatarski, *Wave Propagation in a Turbulent Medium*, McGraw-Hill Book C. inc., New York, 1961, L. C. Andrews and R. L. Phillips, *Laser Beam Propagation through Random Media*, SPIE Press, Bellingham, 1998, R.L. Fante, "Electromagnetic beam propagation in turbulent media", *Proc. IEEE*, vol. 63, pp. 1669-1692, 1975 and R.L. Fante, "Electromagnetic beam propagation in turbulent media: An update", *Proc. IEEE*, vol. 68, pp. 1424-1443, 1980

[2] M. C. Roggemann and B. Welsh, *Imaging through turbulence*, CRC Press, New York, 1996

[3] J. M. Martin and S. M. Flatté, "Intensity images and statistics from numerical simulation of wave propagation in 3-D random media", *Appl. Optics*, vol. **27**(11), pp. 2111-2126, 1988

[4] W. M Coles, J. P. Filice, and M Yadlowski, "Simulation of wave propagation in three-dimensional random media", *Appl. Optics*, vol. **34**(12), pp. 2089-2101, 1995

[5] H. Jakobsson, "Simulation of time series of atmospherically distorted wave fronts", *Appl. Optics*, vol. **35**(9), pp. 1561-1565, 1996

[6] M. C. Roggemann, B. M. Welsh, D. Montera and T. A. Rhoademer, "Method for simulating atmospheric turbulence phase effects for multiple time slices and anisoplanatic conditions", *Appl. Optics*, vol. **34**(20), pp. 4037-4051, 1995

[7] A. Belmonte, "Feasibility study for the simulation of beam propagation: consideration of coherent lidar performance", *Appl. Optics*., vol. **39**(30), pp. 5426-5445, 2000

[8] O. Steinvall, G. Bolander, L. Sjöqvist et al., "Single and double path link measurements over water", *Proc. SPIE*, vol. 5412, pp. 37-53, 2004

[9] O. Steinvall, G. Bolander, L. Sjöqvist et al., "Predicting laser beam propagation in naval environment", *Proc. SPIE*, vol. 5615, pp. 84-99, 2005

[10] O. Steinvall, G. Bolander, L. Sjöqvist et al., "Laser propagation through turbulence over land and sea", *Proc. SPIE*, vol. 5793, [5793-21], 2005

[11] F. Stromqvist-Vetelino, C. Young, L. Andrews, K. Grant, K. Korbett and B. Clare, "Scintillation: theory vs. experiment", *Proc. SPIE*, vol 5793, pp. 166-177, 2005

[12] S. Benderski, N. Kopeika and N. Blaunstein, "Atmospheric optical turbulence over land in middle east coastal environments: predicition modeling and measurements", *Appl. Optics*, vol. **43**(20), pp. 4070-4079, 2004

[13] S. Benderski, E. Lilos, N. Kopeika and N. Blaunstein, "Modeling and measurements of near ground atmospheric optical turbulence according to weather for Middle East environments", *Proc. SPIE*, vol. 5612, pp. 350-361, 2004

[14] F.M. Davidson, S. Bucaille, G. C. Gilbreath and E. Oh, " Measurements of intensity scintillations and probability density functions of retro-reflected broadband 980-nm laser light in the atmosphere", *Opt. Eng.*, vol. **38**(8), pp. 1288-1295, 1999

[15] J.W. Goodman, *Introduction to Fourier Optics*, 2nd Ed., McGraw-Hill, New York, 1996

[16] A. M. McAulay, "Generating Kolmogorov phase screens for modelling optical tuburbulence", *Proc. SPIE*, vol. 4034, pp. 50-57, 2000

[17] B. L. McGlamery, "Computer simulation studies of compensation of turbulence degraded images", *Proc. SPIE*, vol.74, pp. 225-233, 1976.

[18] T. Goldring and L. Carlson, "Analysis and implementation of non-Kolmogorov phase screens appropriate to structured environment", *Proc. SPIE*, vol. 1060, pp. 244-264, 1989

[19] R. Frelich, "Simulation of laser propagation in a turbulent atmosphere", *Appl. Optics*, vol. **39**(3), pp. 393-397, 2000

[20] G. Sedmak, "Implementation of fast-Fourier-transform-based simulations of extra large atmospheric phase and scintillation screens", *Appl. Optics*, vol. **43**(23), pp. 4527-4538, 2004

[21] C. M. Harding, R. A. Johnston, and R. G. Lane, "Fast simulation of a Kolmogorov phase screen", *Appl. Optics*, vol. **38**(11), pp. 2161-2170, 1999

[22] B. Welsh, "A Fourier Series Based Atmospheric Phase Screen Generator for Simulating Anisoplanatic Geometries and Temporal Evolution", *Proc. SPIE*, vol. 3125, pp. 327-338, 1997

[23] GLAD ver. 5.0, Applied Optics Research Inc., USA, http://www.aor.com, 2005

[24] O. Steinvall, "Performance of laser tracking of small targets during turbulence and beam jitter", *Opt. Eng*., vol. **43**(6), pp. 1609-1621, 2004.